Journal of Magnetic Resonance 211 (2011) 195–206

Contents lists available at ScienceDirect

Journal of Magnetic Resonance

journal homepage: www.elsevier.com/locate/jmr

Experimental aspects in acquisition of wide bandwidth solid-state MAS NMR spectra of low-γ nuclei with different opportunities on two commercial NMR spectrometers

Hans J. Jakobsen [a,*], Henrik Bildsøe [a], Zhehong Gan [b], William W. Brey [b]

[a] Instrument Centre for Solid-State NMR Spectroscopy and Interdisciplinary Nanoscience Center (iNANO), Department of Chemistry, Aarhus University, DK-8000 Aarhus C, Denmark
[b] National High Magnetic Field Laboratory, Florida State University, 1800 East Paul Dirac Drive, Tallahassee, FL 32310, USA

ARTICLE INFO

Article history:
Received 14 March 2011
Revised 25 May 2011
Available online 2 June 2011

Keywords:
Solids low-γ nuclei
Wide-bandwidth NMR spectra
^{14}N MAS NMR
Varian/Bruker spectrometers
Preamplifiers
Electronic evaluations
STARS fitting/simulations
Instrumental parameters
Spectral parameters

ABSTRACT

The acquisition and different appearances observed for wide bandwidth solid-state MAS NMR spectra of low-γ nuclei, using ^{14}N as an illustrative nucleus and employing two different commercial spectrometers (Varian, 14.1 T and Bruker, 19.6 T), have been compared/evaluated and optimized from an experimental NMR and an electronic engineering point of view, to account for the huge differences in these spectra. The large differences in their spectral appearances, employing the recommended/standard experimental set-up for the two different spectrometers, are shown to be associated with quite large differences in the electronic design of the two types of preamplifiers, which are connected to their respective probes through a 50 Ω cable, and are here completely accounted for. This has led to different opportunities for optimum performances in the acquisition of nearly ideal wide bandwidth spectra for low-γ nuclei on the two spectrometers by careful evaluation of the length for the 50 Ω probe-to-preamp cable for the Varian system and appropriate changes to the bandwidth (Q) of the NMR probe used on the Bruker spectrometer. Earlier, we reported quite distorted spectra obtained with Varian *Unity* INOVA spectrometers (at 11.4 and 14.1 T) in several exploratory wide bandwidth ^{14}N MAS NMR studies of inorganic nitrates and amino acids. These spectra have now been compared/evaluated with fully analyzed ^{14}N MAS spectra correspondingly acquired at 19.6 T on a Bruker spectrometer. It is shown that our upgraded version of the STARS simulation/iterative-fitting software is capable of providing identical sets for the molecular spectral parameters and corresponding fits to the experimental spectra, which fully agree with the electronic measurements, despite the highly different appearances for the MAS NMR spectra acquired on the Varian and Bruker spectrometers.

1. Introduction

During the course of the past decade our two laboratories (Aarhus University and the NHMFL, Tallahassee) and other groups have been heavily engaged in developments of experimental technique for the observation of wide bandwidth solid-state NMR spectra of low-γ quadrupolar nuclei, in particular for the ^{14}N quadrupolar nucleus (spin $I = 1$ and 99.3% natural abundance). Clearly, the aim of these developments has been the possibility for a determination of ^{14}N quadrupolar coupling constants and asymmetry parameters (C_Q and η_Q) and, if present, combined with a simultaneous determination of ^{14}N chemical shift anisotropy (CSA) parameters, i.e., the chemical shift anisotropy (δ_σ), asymmetry parameter (η_σ), and relative tensor orientation, from solid-state NMR of polycrystalline powders. These techniques involve methods for the direct detection of reliable wide bandwidth solid-state ^{14}N magic-angle spinning (MAS) [1–9] and impressively WURST-QCPMG sensitivity-enhanced ^{14}N static [10–12] NMR spectra, as well as indirect detection employing two-dimensional MAS methods with observation of ^{13}C or ^{1}H in directly bonded ^{13}C–^{14}N or ^{1}H–^{14}N systems [13–23]. Using direct ^{14}N MAS NMR observation, the obtained spectra not only allow determination of high-precision values for the ^{14}N C_Q and η_Q parameters with magnitudes of C_Q up to $C_Q = 1.3$ MHz (e.g., as illustrated for a series of amino acids [4] or other RNH_3^+ samples [7] of polycrystalline powders), but also of the ^{14}N δ_σ and η_σ parameters (e.g., for nitrates [1,5] and some tetraalkylammonium salts [3]). However, employing indirect two-dimensional techniques, ^{14}N quadrupolar coupling constants for some of the amino acids [4] and most importantly for the amide bonds (–CO–NH–) in selected small peptides with magnitudes up to $C_Q = 2$–3 MHz, have been determined [13–23].

As is evident from the studies on direct observation of ^{14}N MAS NMR spectra [1–9], employing a Varian *Unity* INOVA-600 (14.1 T)

* Corresponding author. Fax: +45 8619 6199.
E-mail address: hja@chem.au.dk (H.J. Jakobsen).

1090-7807/$ - see front matter © 2011 Elsevier Inc. All rights reserved.
doi:10.1016/j.jmr.2011.05.015

spectrometer, we have been faced with several experimental challenges during the course of our research; however, some of these have been successfully overcome. Perhaps the most striking example is evident already from our first report on ^{14}N MAS NMR [1], which shows that an unusually low value for the rf bandwidth (*rfbw*) of only ~0.2 MHz must be adopted in order to achieve optimum simulated fits to the experimental ^{14}N MAS spectra of nitrate ions (NO_3^-). According to the expression $rfbw = \upsilon_0/Q$, where υ_0 is the Larmor frequency and Q is the quality factor of the probe, the low *rfbw* value was at that time [1] therefore mainly ascribed to the low Larmor frequency (υ_0 = 43.34 MHz) for ^{14}N at 14.1 T. Accordingly, this would correspond to a somewhat high value for the probe Q, i.e., $Q = \upsilon_0/rfbw = 43.34/0.2 = 217$. Another experimental factor, which could contribute to the suppression of the heights (''apparent intensities'') for the spinning sidebands (ssbs) in the outer wings of the ssb manifold, is spinning instability in the MAS spinning frequency (υ_R) as has recently been demonstrated to occur for spinning instabilities as low as $\Delta\upsilon_R \sim \pm 0.5$ Hz, depending on the line widths within the lineshapes for the individual ssbs of the manifold of ssbs [9]. However, spinning instability has not been an issue in our ^{14}N MAS NMR studies, e.g., for the nitrate ions [1,2,4–6]. On the contrary, the extremely well-resolved lineshape patterns within the individual ssbs of the ssb manifold for the nitrates have allowed the first determination of CSA data from consideration of the second-order cross-term between the quadrupole coupling and chemical shift interactions [1,2,5,6].

Apparently, the extensive suppression of ssbs in the wings of wide bandwidth ^{14}N MAS NMR spectra acquired on Varian *Unity* INOVA spectrometers appears not to be unique for our Varian spectrometer since results reported by other Varian users show the same effect of a very narrow *rfbw*. For example, the ^{14}N MAS NMR spectrum of L-alanine reported by Khitrin and Fung [24], acquired on a Varian INOVA-500 spectrometer using a spinning frequency υ_R = 5.3 kHz, displays only about 15 ssbs (i.e., a total width of approximately 80 kHz). This corresponds to detection of only the central part of the more than tenfold larger width (approximately 1.2 MHz) observed more recently for L-alanine in our ^{14}N MAS NMR investigation of the simple amino acids [4]. Most importantly, in that study [4] it was demonstrated that the main reason for the increase in *rfbw* to values >1 MHz results from simply removing any 50 Ω low- or band-pass filter in the coaxial cable between the observe channel of the probe and the input to the Varian High-Power (HP) preamplifier. This increase in *rfbw* to $\geqslant$1 MHz corresponds to a decrease in the ''apparent'' probe $Q = \upsilon_0/rfbw \leqslant 43.34/1 \sim \leqslant 43$. These dramatic changes in the ''apparent'' Q of the probe, depending on the experimental coax-cable/filter set-up, also differ widely from the actually measured Q = 130 provided by the manufacturer, and are further explored/accounted for in the present study in relation to the Varian HP preamplifier.

Following the ^{14}N MAS study of the amino acids [4] we were approached by researchers from the National High Magnetic Field Lab (NHMFL), Tallahassee [25], who had performed direct observation of ^{14}N MAS NMR spectra at 19.6 T (60.2 MHz) on a Bruker 830-DRX spectrometer also for glycine and L-alanine, but obtained spectra of quite different appearances compared to those published [4], and for that reason were not subjected to analysis. In this work we investigate the reasons and give some distinct explanations for the different appearances of wideband (low-γ) ^{14}N MAS NMR spectra acquired on Varian and Bruker spectrometers, present excellent analyses and simulations of the Bruker ^{14}N MAS spectra, and most importantly give some further useful hints for improving the experiments. Finally, a detailed electronic analysis of the two preamplifiers, in particular for that of the Varian HP preamp, has been performed and the results are compared. These data reveal some new and different opportunities for the acquisition of wide bandwidth MAS NMR spectra of low-γ nuclei on Varian and Bruker spectrometers.

2. Experimental

2.1. Materials

The samples of lead nitrate ($Pb(NO_3)_2$), glycine, and L-alanine used in this work are all commercially available and were used without further purification.

2.2. ^{14}N MAS NMR spectroscopy

^{14}N MAS NMR experiments were performed on a Varian *Unity* INOVA-600 spectrometer (14.1 T) at 43.34 MHz, Aarhus University and on a Bruker 830-DRX spectrometer (19.6 T) at 60.20 MHz, National High Magnetic Field Lab, Florida State University (FSU), Tallahassee.

2.2.1. Varian Unity INOVA-600 spectrometer

This spectrometer was equipped with a wide-bore Oxford magnet and employed a Varian/Chemagnetics low-γ broadband-frequency 7.5 mm T3® CP/MAS probe based on transmission-line-tuning technology for the ^{14}N experiments at 43.34 MHz. The probe has a maximum spinning frequency of 7 kHz and its spinning frequency is stabilized to <±0.5 Hz for the 7.5 mm zirconia rotor using the Varian/Chemagnetics MAS speed controller, as recently demonstrated [9]. The magic angle of θ = 54.736° was adjusted to the highest possible precision (i.e., $\Delta\theta$ < ±0.003°) employing the ^{14}N MAS NMR spectrum of $Pb(NO_3)_2$ [5]; however, upon sample (rotor) change, the angle may change by up to >±0.005° as judged from computer simulations of the spectra. The ^{14}N chemical shift δ-scale is referenced to the narrow resonance, FWHM (Full Width at Half Maximum) ~0.3 ppm, for an external sample of solid NH_4Cl. Generally, spectra were acquired with a coaxial cable straight between the observe channel of the probe and the preamp (i.e., with no low- or band-pass filter inserted in the line) in order to observe almost undistorted spectra with a bandwidth of almost 2 MHz [4]. Different lengths of coaxial cables were tested to obtain optimum wideband performances for these experiments (*vide supra*). This set-up, without any filters in the observe line, prohibits use of the ^{1}H decoupler channel during acquisition, a technique not required for reducing line widths in the ^{14}N MAS spectra studied in this work [4]. However, for RNH_3^+ samples requiring spinning frequencies υ_R < 3 kHz and therefore ^{1}H decoupling [7–9], we designed two pieces of 600 MHz LC-series ''traps-to-ground'' (each built into a Pomona box and providing an isolation of 31 dB, for a total measured isolation of 63 dB at 600 MHz). These may be inserted into a coaxial cable, giving a total length identical to the optimum cable length, and thereby effectively suppresses any 600 MHz ''noise'' frequency leaking through the probe ^{1}H decoupler circuitry into the observe channel (*vide supra*), while still achieving optimum wideband performances. Excitation and acquisition of the ^{14}N MAS NMR spectra employed single-pulse excitation, a (liquid) flip angle of ~15°, i.e., τ_p = 1 μs (τ_p^{90} = 6.3 μs), a spectral width of 2 MHz, a spinning frequency υ_R = 6000 Hz, and a repetition delay of 2 s. The number of scans ranged from 16,000 for the ^{14}N MAS spectra of $Pb(NO_3)_2$ to 120,000 scans for the two amino acids, which correspond to spectrometer times of approximately 9 h and 3 days, respectively.

2.2.2. Bruker 830-DRX spectrometer

This spectrometer is equipped with a special narrow-bore (31 mm i.d.) 19.6 T Magnex magnet and employed a homebuilt (NHMFL) broadband-frequency 4 mm single-resonance MAS probe (29 mm o.d.), which uses 4 mm Bruker rotors [26]. The ^{14}N MAS

experiments were performed at 60.20 MHz and employed a spinning frequency υ_R = 10 kHz, however, without stabilization of υ_R by a spinning-speed controller and without the use of ^{1}H decoupling. On this spectrometer, the magic angle of θ = 54.736° was adjusted using the actual sample of glycine by optimizing to the most narrow line width (FWHM) for the individual ssbs. We find that at the increased magnetic field strength of 19.6 T, the second-order quadrupolar line broadening of the ssbs has decreased considerably, as expected [27,28], from FWHM ~700 Hz observed earlier at 14.1 T (43.3 MHz) [4] to FWHM ~350 Hz determined following the magic-angle adjustment at 19.6 T (60.2 MHz); Note: According to simulations, the 19.6 T value of 350 Hz actually corresponds to a slightly off-MAS condition of $\Delta\theta = -0.018°$ while for exactly on-MAS adjustment ($\Delta\theta = 0°$) the simulations show that FWHM ~475 Hz, *vide supra*. This allows each spectrum in the angle-adjustment procedure to be recorded within 5 min (i.e., each spectrum required 3000 scans with a repetition delay of 0.1 s). Since deviations from the achieved angle setting readily occur upon changes of sample rotors, as e.g. observed for the spectrum of L-alanine recorded in this work, it is a clear advantage if the magic angle can be adjusted directly on the sample to be investigated. No special attention had to be paid to the length of the coaxial cable between the probe and the Bruker preamplifier in the acquisition of the ^{14}N MAS NMR spectra (*vide supra*). Excitation and acquisition of the ^{14}N MAS NMR spectra employed single-pulse excitation, a (liquid) flip angle of 20°, i.e., τ_p = 1 μs (τ_p^{90} = 4.5 μs or $\gamma B_1/2\pi$ = 55.6 kHz), a spectral width of 1 MHz, a spinning frequency υ_R = 10 kHz, a relaxation delay of only 0.1 s, and the number of scans between 10,240 and 24,000 (i.e., between 20 and 40 min for each spectrum). It is noted that on this spectrometer, the spectral width is limited to 1.0 MHz, which corresponds to the maximum digitization rate for the receiver.

2.3. Simulation of ^{14}N MAS NMR spectra

All spectra were analyzed by computer simulation/iterative fitting on a Sun Microsystem Ultra-5 workstation or on a Linux RedHat PC using the STARS solid-state NMR software package developed in our laboratory and incorporated into either the Varian VNMR or VNMRJ software [28,29]. Several new features have been incorporated into the STARS software in order to fully appreciate the effects of the many experimental factors associated with ^{14}N MAS NMR (e.g., magic-angle adjustment and spinning-speed stability), as has also been discussed elsewhere [4,9], and were included in the fitting process. In particular we note that the present version of STARS can simultaneously handle up to eight different nuclear sites in an iterative fit to an experimental spectrum. The quadrupolar coupling parameters employed in the simulations using STARS are related to the principal elements of the electric-field gradient tensor ($\boldsymbol{V}$) by

$$C_Q = eQV_{zz}/h \tag{1}$$

$$\eta_Q = (V_{yy} - V_{xx})/V_{zz} \tag{2}$$

where the principal tensor elements are defined by

$$\begin{aligned} &V_{xx} + V_{yy} + V_{zz} = 0 \\ &|V_{zz}| \geqslant |V_{xx}| \geqslant |V_{yy}| \end{aligned} \tag{3}$$

Because of the negligibly small ^{14}N CSA apparent from ^{14}N MAS spectra of amino acids [4] and other RNH_3^+ samples [7], this interaction is also neglected in the simulations of the 19.5 T spectra for the amino acids. However, ^{14}N CSA is fairly large in nitrates, where it has a pronounced effect on the appearances of the lineshapes for the ssbs [1,2,5], and is therefore taken into account in the simulation of the spectra for $Pb(NO_3)_2$. The ^{14}N CSA parameters (δ_σ, η_σ, and the relative tensor orientation) determined and used by STARS for $Pb(NO_3)_2$ are related to the principal elements of the chemical shift tensor by $\delta_\sigma = \delta_{iso} - \delta_{zz}$, $\eta_\sigma = (\delta_{xx} - \delta_{yy})/\delta_\sigma$, $\delta_{iso} = (\delta_{xx} + \delta_{yy} + \delta_{zz})/3$ where $|\delta_{zz} - \delta_{iso}| \geqslant |\delta_{xx} - \delta_{iso}| \geqslant |\delta_{yy} - \delta_{iso}|$. Finally, the simulations of the 14.1 T $Pb(NO_3)_2$ ^{14}N MAS NMR spectra employed an infinitely strong excitation pulse as used earlier [1,4], while for the 19.6 T ^{14}N MAS spectra of glycine and L-alanine a finite or short excitation pulse (defined by $\gamma B_1/2\pi$ and pw) was employed. The reported *rfbw* values correspond to measurements at a point 3 dB down from the top of the resonance peak (−3 dB), i.e., at a position of ~75% of the peak height.

2.4. Electronic measurements of NMR-preamplifier bandwidths

The bandwidths of the Varian and Bruker preamplifier systems and the detailed frequency dependence of their system gain were evaluated using two different methods of electronic measurements. In one case this was done by measurements of the complex input impedance for the respective preamplifier and the probe. In the second and in practice somewhat simpler case, we directly measured the frequency dependent gain of a small test signal injected into the probe and amplified by the preamp. It is noted that if a multi-channel probe is in use, it may be possible to use one of its other channels to inject the test signal into its tuned/matched observe channel. Parameters such as the length of cable between the probe and preamp were varied and observed to change the bandwidth over a fairly wide range for the Varian preamp. The two measurements were performed on typical solid-state NMR instruments from both Varian (14.1 T, ^{14}N at 43.3 MHz) and Bruker (19.6 T, ^{14}N at 60.20 MHz). For the Varian system we used a Varian High-Power (HP) broadband preamp intended for solid-state NMR. The 43.3 MHz frequency was injected into one of the separate ports (not tuned/matched to 43.3 MHz) on a standard 14.1 T Varian triple-resonance probe, however, with the observe port tuned/matched to ^{14}N at 43.3 MHz. For the very narrow (29 mm o.d.) homebuilt 4 mm single-resonance MAS probe used for the 19.6 T Bruker ^{14}N (60.20 MHz) MAS NMR experiments, a test signal was directly injected into the tuned/matched observe coil using a small external coil positioned inside the probe. Measurements of the gain for both systems were conducted using an Agilent 8753ES Vector Network Analyzer (VNA). The VNA was calibrated using the standard short-open-load-thru (SOLT) method out to the end of the cable. The *rfbw* and probe-*Q* values are for −3 dB down from the top of the curves, similar to the *rfbw* values reported from the spectral simulations.

3. Results and discussion

3.1. ^{14}N MAS NMR spectroscopy on Varian and Bruker spectrometers

As mentioned in the introduction, demonstrated earlier experimentally [4], and shown in Fig. 1, a prerequisite for the observation of "ideal" wide bandwidth solid-state ^{14}N MAS NMR spectra (or of other low-γ nuclei) employing a Varian *Unity* INOVA spectrometer is to use a coaxial cable (without any low- or band-pass filter) straight between the probe and high-power preamplifier and of appropriate length. Thus, to perform ^{1}H decoupling without any degradation in S/N ratio, resolution or loss of the wideband performance, insertion of the two 600 MHz LC traps (described in Section 2) in the observe line is required. The effect on the performance is illustrated in Fig. 2 using the highly resolved spectrum of $Pb(NO_3)_2$ as an example. The ^{14}N MAS NMR spectrum in Fig. 2 (upper) is that of $Pb(NO_3)_2$ acquired without ^{1}H decoupling, while that in Fig. 2 (lower) is acquired by turning the ^{1}H decoupler on with an rf field strength of 50 kHz. A comparison shows that the two spectra appear identical with no degradation first of all in

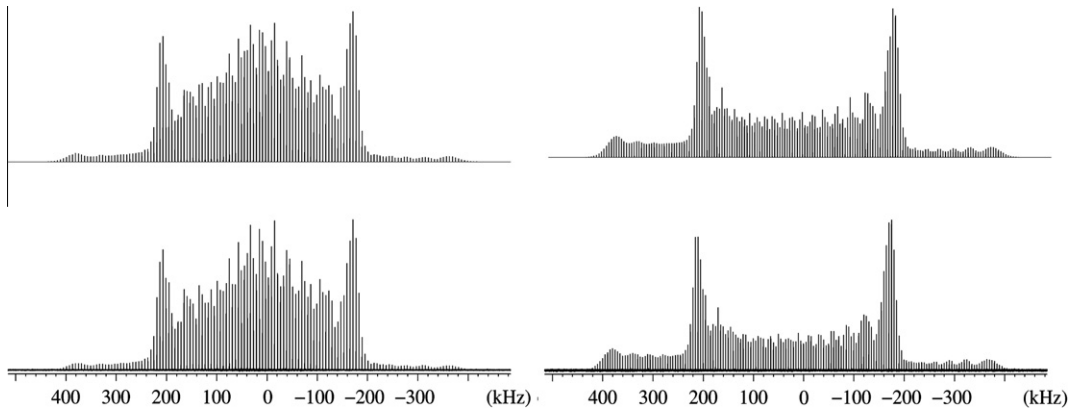

Fig. 1. 43.34 MHz (14.1 T) experimental (lower row) and corresponding simulated (upper row) ^{14}N MAS NMR spectra of $Pb(NO_3)_2$ for υ_R = 6000 Hz. The spectra to the left employed a K&L low-pass filter in the coaxial cable between the probe and the Varian preamplifier, and from the optimized fit to the experimental spectrum this results in a value for *rfbw* = 0.2 MHz and a value $\Delta\theta = -0.002°$ for the deviation from exact setting of the magic angle. For the spectra to the right the K&L low-pass filter has been removed from the coaxial cable, and from the optimized fit to the experimental spectrum *rfbw* = 0.9 MHz and $\Delta\theta = -0.005°$ were obtained. The spectral parameters (C_Q = 539 kHz, η_Q = 0.01, δ_σ = 149 ppm, η_σ = 0.00, δ_{iso} = 334.5 ppm) determined from the optimized fits to the two experimental spectra are identical and within the error limits of those earlier reported for $Pb(NO_3)_2$ [1,5].

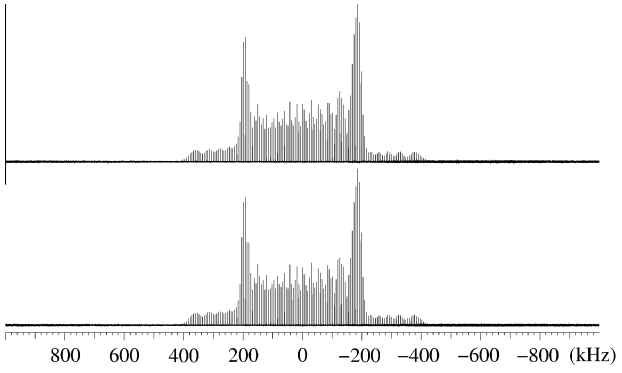

Fig. 2. 43.34 MHz (14.1 T) experimental ^{14}N MAS NMR spectra of $Pb(NO_3)_2$ for υ_R = 6000 Hz, acquired without (upper) and with (lower) ^{1}H decoupling (50 kHz rf field strength) using two identical, homebuilt pieces of 600 MHz LC-series "traps-to-ground" in the observe line between the probe and Varian HP preamp, as opposed to a low- or band-pass filter. Note the identical noise levels for the two baselines, and that the wide bandwidth is retained in the spectra (cf. Fig. 1 and see the text).

noise level or in resolution caused by the ^{1}H decoupling. Moreover, comparison with the ^{14}N MAS spectra of $Pb(NO_3)_2$ in Fig. 1, using a coaxial cable (without filter or traps) straight between the probe and preamp, indicates that the wide bandwidth performance is retained for the two spectra in Fig. 2. The slight difference in the "tilt" of the intensities for the two "horns" in the spectra of Fig. 2, compared to those in Fig. 1 or those in the figures of references [4,5], is caused by a combination of a slight difference in the length used for the two setups of the coaxial cables (with and without traps) and a slight deviation in the magic-angle adjustments. Spectral analysis of the two spectra in Fig. 2 yields identical parameter sets for C_Q, η_Q and δ_σ, η_σ, and identical to those determined for the spectra in Fig. 1.

The extreme influence of the length for the observe coaxial cable between the probe and the Varian HP preamp on the ^{14}N MAS NMR spectra is illustrated in Fig. 3, using $Pb(NO_3)_2$ as a test sample once again. The almost ideal, undistorted spectrum in Fig. 3 (upper) is observed for a cable length of 210 cm, whereas highly distorted spectra (tilted with a quite small reduced *rfbw*) are obtained for cable lengths of 236 cm, Fig. 3 (lower left) and 192 cm, Fig. 3 (lower right). The latter two spectra correspond to a high- and low-frequency rf offset, respectively, combined with the quite small reduction in the bandwidths of the two spectra. The observed extremely high sensitivity of the spectral tilting on quite small variations in the length of this cable for ^{14}N observe at 43.34 MHz contrasts the much less pronounced dependence observed for higher-frequency nuclei on the same spectrometer, e.g., for ^{11}B (192.50 MHz), ^{23}Na (158.71 MHz), and ^{27}Al (156.34 MHz). It is noted, as mentioned elsewhere [4,7–9], that the same tilting-effect on the high- and low-frequency ssb intensities can alternatively be compensated for by changing/optimizing the length of the adjustable so-called $\lambda/4$ wavelength cable on the Varian preamp. However, because these $\lambda/4$ preamp cables are primarily intended for optimized performance and serve as protection/isolation of the preamp circuitry, we recommend the Varian Users to stick to Varian's guidelines regarding the appropriate use of the $\lambda/4$ cables for their different frequency ranges, and instead optimize the tilting/offset effects through the length of the coaxial cable directly between the probe and preamp.

Now, for a comparison of the ^{14}N MAS NMR spectra discussed and illustrated above for glycine and $Pb(NO_3)_2$, respectively, and acquired at 14.1 T (43.34 MHz) on the Varian *Unity* INOVA-600 spectrometer, the ^{14}N MAS spectra acquired for glycine at 19.6 T (60.20 MHz) on the Bruker 830-DRX spectrometer will be presented. Two different sets of glycine ^{14}N MAS NMR spectra, acquired under identical rf conditions but at very different dates on the 830-DRX spectrometer at the NHMFL, have been subjected to detailed analysis using STARS. The first set (I) of spectra, recorded shortly after publication of the study on the amino acids [4], shows little resemblance to the published spectrum of glycine [4], and for that reason was not subjected to spectral analysis back at that time. The second set (II) of glycine spectra from the Bruker system has recently been obtained, following the start of the present collaboration to resolve the issues resulting in the different appearances between ^{14}N MAS NMR spectra acquired on the Varian *Unity* INOVA-600 and Bruker 830-DRX spectrometer. In order to check the reproducibility of the set (I) spectra several experimental parameters, which potentially may affect the spectral appearance (e.g., magic-angle adjustment, spinning-frequency stability, length of coaxial cable, and rf field-strength calibration), have been optimized before acquisition of the final set (II) glycine ^{14}N MAS NMR spectra. Most importantly, these optimizations immediately show that variations in the lengths of the coax cable between the probe and the Bruker preamp have no (or very little) effect on the 'tilting' of the spectra (*vide supra*), in sharp contrast to what is observed in Fig. 3 for the Varian *Unity* INOVA spectrometer.

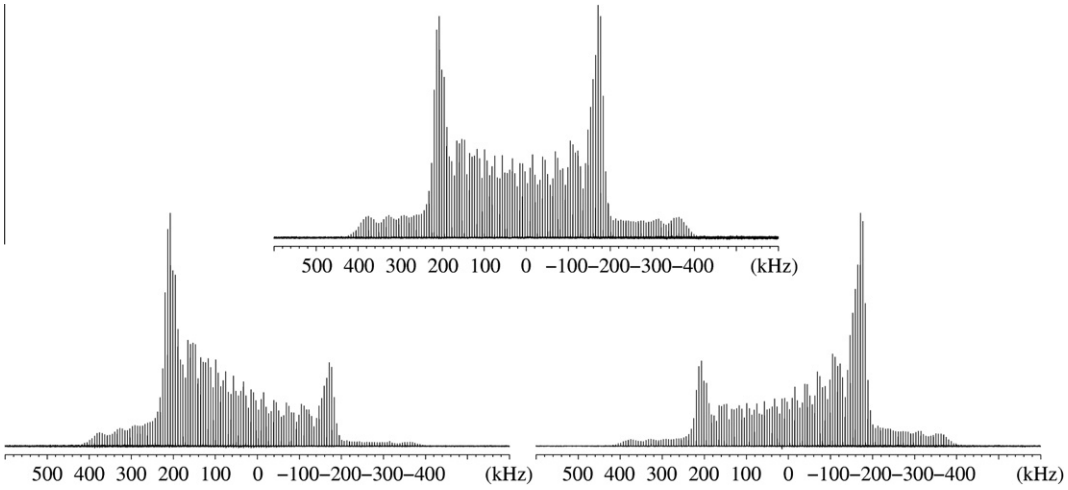

Fig. 3. 43.34 MHz (14.1 T) experimental ^{14}N MAS NMR spectra of $Pb(NO_3)_2$ for υ_R = 6000 Hz, acquired for different lengths of the coaxial cable between the probe and Varian HP preamp, and with no low- or band-pass filter in the line. The upper ideal spectrum is obtained for a length of 210 cm, while the two lower, highly intensity distorted spectra (however, quite symmetrically distorted) were obtained for cable lengths of 236 cm (lower left) and 192 cm (lower right).

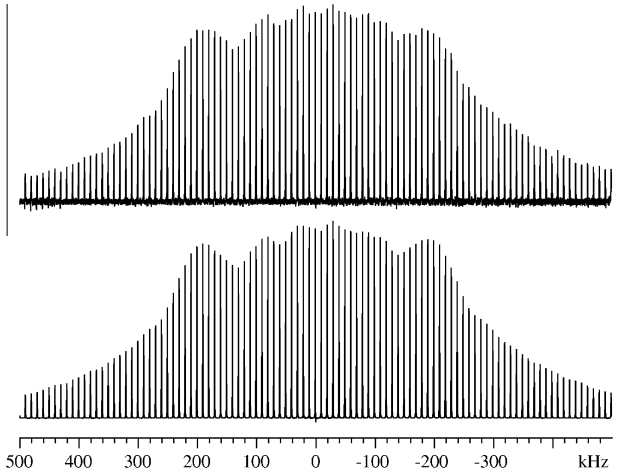

Fig. 4. Set (I) Bruker 60.20 MHz (19.6 T) ^{14}N MAS NMR experimental (upper) and simulated (lower) spectrum of glycine for υ_R = 10 kHz, a spectral width of 1.0 MHz (maximum available), and 10,240 scans with a relaxation delay of 0.1 s (i.e., a spectrometer time of 17 min). The spectral analysis and the spectral parameters resulting from the optimized fit (lower spectrum) to the experimental spectrum are presented in the text.

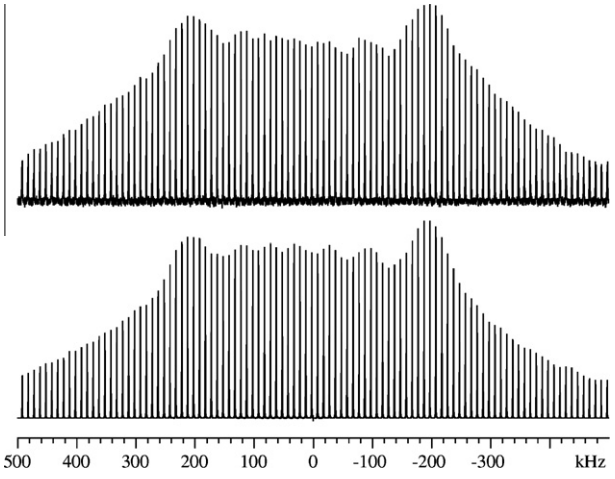

Fig. 5. Set (II) Bruker 60.20 MHz (19.6 T) ^{14}N MAS NMR experimental (upper) and simulated (lower) spectrum of glycine acquired several years later than that for the set (I) spectrum, but for the exactly identical experimental conditions as shown in Fig. 4, except that the magic angle has been optimized on the glycine sample (see Section 2), just prior to recording the upper spectrum. The spectral analysis and the spectral parameters resulting from the optimized fit (lower spectrum) to the experimental spectrum are presented in the text.

As an illustrative example of the set (I) 19.6 T glycine ^{14}N MAS NMR spectra obtained on the Bruker spectrometer, Fig. 4 shows a glycine spectrum acquired employing the maximum spectral width of 1.0 MHz available for this spectrometer and after 10,240 scans (17 min of spectrometer time). At the time when the spectrum was first discussed in the context of the present collaboration, it was obvious that this spectrum shows considerably fewer distortions with respect to suppression of the ssb intensities towards the wings of the spectrum, when compared to the distortions observed in our [4] and others [24] first attempts to acquire ^{14}N MAS NMR spectra of the amino acids on Varian *Unity* INOVA spectrometers and also to our initial ^{14}N MAS NMR investigations [1,2]. As an example of the recently observed set (II) ^{14}N MAS NMR spectra of glycine, acquired following careful optimizations of the experimental parameters (*vide infra*), Fig. 5 shows the spectrum obtained again after 10,240 scans (17 min). Comparison with the experimental spectrum in Fig. 4 shows that the ssbs in the region for the two "horns" (characteristic of the published spectrum of glycine; cf Fig. 4 in Ref. [4]) appear with an overall higher "apparent" intensity in the Fig. 5 spectrum (it is noted that the *integrated* intensities are equal for these ssbs in the two spectra). We ascribe the observed different appearances of the spectra in Figs. 4 and 5 to an improved stability in spinning frequency during acquisition of the spectrum in Fig. 5 ($\Delta\upsilon_R$ < ±2 Hz as read off from a frequency counter during the 34 min period of the experiment) compared to a spinning instability of $\Delta\upsilon_R$ = ±5 Hz noted for the set (I) spectra (e.g., Fig. 4). (Note: The Bruker 830-DRX spectrometer at the NHMFL is not equipped with a MAS speed controller).

Despite some limitations in the experimental set-up (i.e., max. spectral window of 1.0 MHz and no MAS speed controller) for acquisition of the wide bandwidth ^{14}N MAS NMR spectra characteristic for the amino acids, attempts have been made to extract the spectral parameters (C_Q, η_Q, and δ_{iso}) from the two sets of spectra acquired at 19.6 T in Figs. 4 and 5 as well as the experimental parameters (υ_R, $\Delta\upsilon_R$, *rfbw*, $\Delta\theta$, *rfoffset*) affecting these spectra. These attempts were successfully performed using the most recently updated versions of our STARS solid-state NMR simulation/fitting software-package (see Section 2.3) and involved

independent fitting of simulated spectra to the individual experimental spectra through variations of the eight parameters listed above along with a Lorentzian line width for the ssbs. The resulting optimized simulated spectra are displayed below their corresponding experimental spectra in Figs. 4 and 5 and both show an excellent agreement with their respective experimental partner. Because of the limited spectral window of 1.0 MHz, a fold-in of a few low-intensity ssbs are sometimes observed in the experimental Bruker spectra, as e.g. observed in the region 440–500 kHz for the experimental spectrum of Fig. 4. However, these minute intensities of fold-in ssbs do not affect the simulations since these ssbs can be excluded in the STARS fitting procedure. The corresponding spectral and experimental parameters obtained for the optimized fitted sets (I) and (II) spectra in Figs. 4 and 5 are from Fig. 4: $C_Q = 1.17 \pm 0.02$ MHz, $\eta_Q = 0.52 \pm 0.02$, $\delta_{iso} = -6.1 \pm 0.5$ ppm, $\upsilon_R = 9990$ Hz, $\Delta\upsilon_R = \pm 5$ Hz, *rfbw* = 750 ± 60 kHz, $\Delta\theta = 0.008°$, *rfoffset* = −14 kHz, and from Fig. 5: $C_Q = 1.17 \pm 0.02$ MHz, $\eta_Q = 0.51 \pm 0.02$, $\delta_{iso} = -6.0 \pm 0.5$ ppm, $\upsilon_R = 9994$ Hz, $\Delta\upsilon_R = \pm 1.0$ Hz, *rfbw* = 750 ± 60 kHz, $\Delta\theta = -0.018°$, *rfoffset* = 31 kHz. It is most encouraging that the spectral parameters C_Q, η_Q, and δ_{iso} determined from both sets of spectra are completely identical to the corresponding data reported [4] and determined from the Varian *Unity* INOVA-600 spectrometer (14.1 T). In addition to the excellent spectral fits of the overall ssb manifolds illustrated in Figs. 4 and 5, the high quality of the fitting procedure involving all the parameters listed above can be further appreciated from a comparison of the experimental and simulated individual line shapes illustrated in Fig. 6, obtained from expansion of a selected region for the ssb manifold in the Fig. 5. Comparison of the experimental, magic-angle adjusted spectrum in Fig. 6 (upper), adjusted by minimizing the FWHM of the ssbs with the $\Delta\theta$-fitted spectrum in Fig. 6 (middle) (giving $\Delta\theta = -0.018°$) and the simulated $\Delta\theta = 0.000°$ spectrum in Fig. 6 (lower), illustrates the power of the STARS program, and that a minimum value for the FWHM of the ssbs is not always the optimum criterion for the exact setting of the magic angle ($\Delta\theta = 0.000°$).

As a final demonstration of the reliable and convincing set of parameters extracted above from the two sets, (I) and (II), of Bruker spectra, we have taken advantage of these parameters in a direct simulation (no optimized fitting) for a pw-array series from the old set (I) of Bruker spectra for glycine (pw = 1.0, 1.5, 2.0, 2.5, 3.0, and 3.5 μs). The experimental and simulated spectra are illustrated in Fig. 7. Similar to the optimized simulation in Fig. 4 a finite pulse (for $\gamma B_1/2\pi = 55.6$ kHz) has been used in these simulations for the different pw values along with the parameters determined from the spectra in Fig. 4 (*vide infra*). Exceptionally good agreements are observed in all cases (Fig. 7) between the experimental and simulated spectra, which are believed to be the first of their kind.

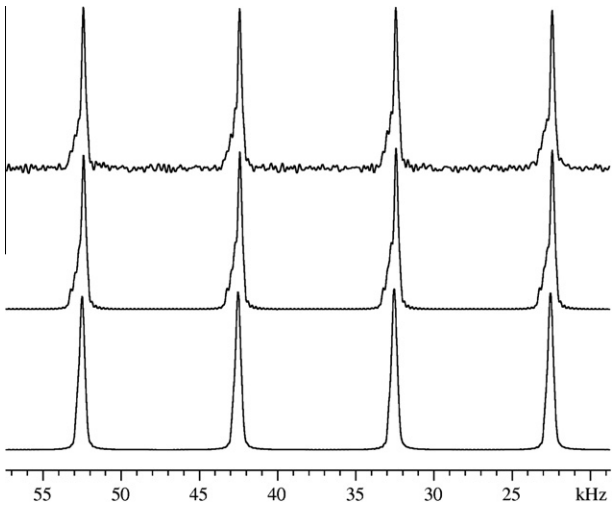

Fig. 6. Expansion of four ssbs in the experimental spectrum (upper) of the set (II) Bruker 60.20 MHz (19.6 T) ^{14}N MAS NMR spectrum of glycine in Fig. 5. Simulation (middle) illustrating the optimized $\Delta\theta$ (deviation from exact magic angle setting) fit to the line shapes of the ssbs in the experimental (upper) spectrum giving $\Delta\theta = -0.018°$. Simulation (lower) illustrating the line shapes of the ssbs for $\Delta\theta = 0.000°$ (see text).

Following the recording of the set (II) Bruker spectrum of glycine (Fig. 5), with an optimized magic-angle setting of $\Delta\theta = -0.018°$ (Fig. 6), it was tempting to take advantage of the optimized experimental conditions and record a ^{14}N MAS spectrum of L-alanine. ^{14}N MAS NMR spectra of L-alanine acquired on Varian *Unity* INOVA spectrometers have earlier been intensively studied and analyzed [4,24], and thus a comparison of these spectra with a wide bandwidth ^{14}N MAS spectrum of L-alanine acquired on the Bruker spectrometer would be of interest. The acquired Bruker ^{14}N MAS spectrum of L-alanine ($\upsilon_R = 9992$ Hz, 24,000 scans in 40 min) is shown in Fig. 8, where the increased intensity tilt of the "horn" at high frequency immediately shows that a change in magic-angle setting has occurred during the sample change of rotors from glycine to L-alanine. Furthermore, a comparison with the experimental and simulated ^{14}N MAS spectra in Fig. 3 of Ref. [4] indicates that the magic-angle setting has changed from a negative deviation ($\Delta\theta = -0.018°$) to a positive deviation ($\Delta\theta > 0°$). Optimized fitting of simulated spectra to the experimental spectrum results in the final simulated spectrum shown in Fig. 8 (lower) and the corresponding final parameters: $C_Q = 1.16 \pm 0.02$ MHz, $\eta_Q = 0.24 \pm 0.02$, $\delta_{iso} = -5.0 \pm 0.5$ ppm, $\upsilon_R = 9992$ Hz, $\Delta\upsilon_R = \pm 1$ Hz, *rfbw* = 870 ± 80 kHz, $\Delta\theta = +0.056°$, *rfoffset* = −30 kHz. Again the spectral parameters (C_Q, η_Q, and δ_{iso}) are within the experimental errors for the values determined earlier from the highly symmetrical wide bandwidth spectrum of L-alanine acquired employing the optimized experimental setups on a Varian *Unity* INOVA spectrometer at 14.1 T [4]. Most interestingly the optimized fit for the magic-angle deviation of $\Delta\theta = +0.056°$ confirms the above predicted positive value for this experimental parameter and the well-known, long-standing, and yet unresolved experimental technical problem in MAS NMR spectroscopy, namely an unpredicted change in exact magic-angle setting upon change of sample rotors (i.e., a deviation in $\Delta\theta$ from exact magic-angle adjustment $\Delta\theta = 0.000°$, which can be adjusted to within ±0.001° employing certain samples [4]).

In conclusion, the most striking and important difference between the original Varian and the Bruker experimental set-up (with both systems including their standard low-/band-pass filters which allow ^{1}H decoupling) for acquisition of the low-γ wide-bandwidth ^{14}N MAS NMR spectra obtained earlier on the Varian *Unity* INOVA (14.1 T) spectrometer [1,2,4] and the spectra reported here for the Bruker (19.6 T) system, is the large difference observed for the *rfbw* values on the two spectrometers: *rfbw* ~200 kHz (Varian; see Section 1) and *rfbw* ~750 kHz (Bruker). It is noted that the low-pass or band-pass filters used on the Varian system are high-performance, 50 Ω impedance filters from either K&L or FSY, which are to be inserted into the coaxial cable between the probe and the Varian broadband HP preamp, whereas on the Bruker system the low-pass filters are built into the different frequency stages of the Bruker preamp. Combined with our earlier observation that simply removing any 50 Ω impedance low- or band-pass filter in the Varian set-up increases the *rfbw* to >1 MHz [4] has prompted us to undertake a detailed investigation and comparison of these two different commercial preamplifier systems. This investigation also includes the effect of the length of the transmission line connecting the probe and the preamp on the receiver bandwidth, an analysis employing the Agilent 8753 ES vector network analyzer and which will be presented below.

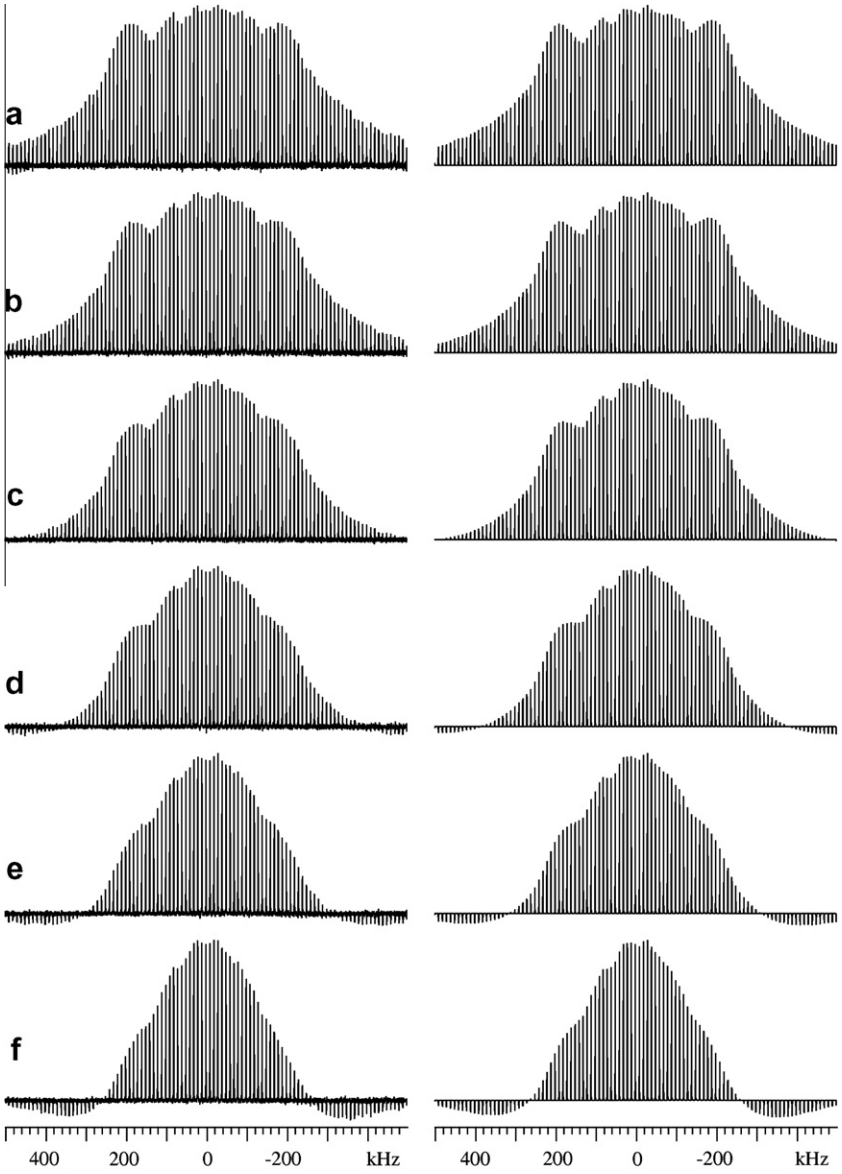

Fig. 7. Experimental spectra (left column) showing a pw-array of the set (I) Bruker 60.20 MHz (19.6 T) ^{14}N MAS NMR spectrum of glycine in Fig. 4 for pw = (a) 1.0, (b) 1.5, (c) 2.0, (d) 2.5, (e) 3.0, and (f) 3.5 μs. The right column shows the corresponding simulated (not fitted) spectra employing the spectral parameters determined for the spectrum in Fig. 4 (see text) and a finite pulse for $\gamma B_1/2\pi$ = 55.6 kHz.

We demonstrate that different opportunities exist for extending the ^{14}N rf bandwidth to ~4 MHz for both systems and point out a straightforward way to characterize and optimize the bandwidth dependence on the length of the transmission line for the Varian system using electronic equipment and software that will be within the capability of many NMR laboratories.

3.2. Electronic characterization of Varian and Bruker preamplifiers for ^{14}N MAS NMR

For the readers interested in the electronic characterization of the Varian and Bruker preamplifiers and also probe design relevant to the experiments presented above, however, unfamiliar with the electronic definitions and calculations discussed below in this section, we refer those readers to some of the details outlined and shown in the Appendix A.

Based on the aforementioned experimental observations we first consider the effect of using a Varian broadband HP preamplifier module on the receiver bandwidth. In an NMR spectrometer and most other types of rf laboratory equipment, sources and loads are transformed to match the 50 Ω characteristic impedance of a low-loss coaxial cable. In such a system, reflections at the ends of the interconnecting cables are very small and can be ignored. However, the input impedance of the Varian preamplifier is significantly different from 50 Ω. Several simplifying assumptions and basic formulas that are used in 50 Ω systems no longer work for the Varian preamplifier. In particular, due to the impedance mismatch between the cable and preamp, the length of the cable between the probe and preamp is found to affect the system bandwidth. The simple formula that relates Q and bandwidth for an NMR probe is no longer reliable, and in fact the bandwidth is found to depend upon the cable length. In fact, for some lengths of the cable between the probe and preamp, the shape of the RF response no longer fits the Lorentzian shape typical of an NMR probe, but has the two peaks that are characteristic of coupled resonances. These differences from the classic response curve can have an important effect on the lineshape analysis of low-γ nuclei with large quadrupolar broadening, so it is important to characterize and understand them.

We have measured the input impedance of a Varian broadband HP preamplifier (the "PROBE" port) from 40 to 46 MHz. The Varian

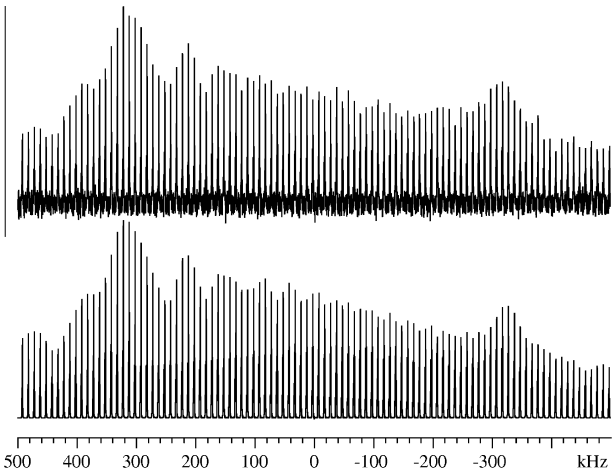

Fig. 8. Bruker 60.20 MHz (19.6 T) ^{14}N MAS NMR experimental (upper) and simulated (lower) spectra of L-alanine with the experimental spectrum acquired immediately following the magic-angle adjustment and recording of the set (II) glycine spectrum in Fig. 5. The spectrum was acquired for $\upsilon_R = 10$ kHz in 40 min (24,000 scans). The spectral analysis and the spectral parameters resulting from an optimized fit (lower spectrum) to the experimental spectrum are presented in the text, where the reason for the tilt of the spectra is also given.

45–65 MHz quarter-wave length cable was in place. At our frequency of interest, 43.3 MHz, the measured impedance is $7 + j14\ \Omega$. Thus, we can model the preamplifier input circuit as a resistor of 7 Ω in series with an inductor of 51 nH (see Appendix A). In the circuit shown in Fig. 9, this corresponds to $R_P = 7\ \Omega$ and $L_P = 51$ nH.

This preamplifier input impedance is in distinction to the simple resistor of 50 Ω that we would typically expect to obtain. However, here it is important to note the transmission line of length L wavelengths between the probe and preamp. For purposes of this discussion, the transmission line is considered to begin at the matching capacitor and include all the fixed lines within the probe body as well as the cable that connects from the probe base to the preamplifier. The components to the left of the transmission line L in Fig. 9 are the familiar sample coil of inductance L_S, the tuning capacitor of capacitance C_T, and matching capacitor of capacitance C_M. Let us propose some typical values for the components of the probe circuit that will produce a resonance at 43.3 MHz which is matched to 50 Ω. Thus, if we take $L_S = 100$ nH, and assume the sample coil has a Q of 50, then the total capacitance $C = C_T + C_M$, required to tune (43.3 MHz) and match the inductor to 50 Ω, is $C = 135$ pF (see Appendix A.1). This result agrees with the values $C_T = 120$ pF and $C_M = 15$ pF obtained using a circuit simulator program or from the formulas used by Anferova et al. [30].

First we consider the behavior that should be expected if the length L of the transmission line is made very much shorter than a wavelength so that its effect can be neglected. The preamp impedance has a real part of 7 Ω and magnitude of 16 Ω, both of which are much less than 50 Ω. The probe has been matched to

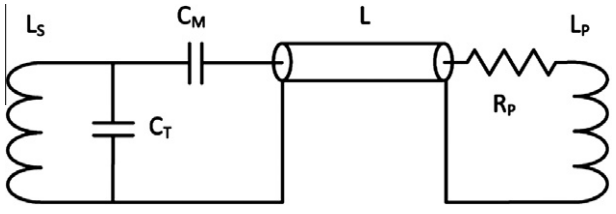

Fig. 9. Electronic circuit for a probe ↔ preamp system referred to in the text for evaluation of the Varian High-Power (HP) preamplifier.

an impedance of 50 Ω, which is larger than the actual load. So it will be undercoupled to the Varian preamp. A probe circuit that is matched to its load will "see" its own parallel impedance through the matching capacitor. An undercoupled circuit will "see" a larger parallel impedance, whereas an overcoupled circuit will "see" a smaller impedance. This parallel impedance will change the circuit Q and bandwidth. In this undercoupled case the Q will be reduced somewhat from the unloaded case, but not by the factor of two obtained for an impedance match. Thus, the bandwidth will be narrower than the matched bandwidth by a factor of between 1 and 2. A circuit simulation indicates that the −3 dB bandwidth is reduced from 1.75 to 1.01 MHz by the undercoupling. We can also calculate the change in bandwidth directly. We take the series combination of C_M, R_P, and L_P and find the equivalent parallel network – at least find the value of the resistive component. We can assume the reactive component is large enough compared to the reactance of L_S that it can be neglected. We can use the well-known series–parallel transformation equations

$$R_{parallel} = \left(R_{series}^2 + X_{series}^2\right)/R_{series} \quad \text{and}$$
$$X_{parallel} = \left(R_{series}^2 + X_{series}^2\right)/X_{series} \tag{4}$$

to determine parallel equivalents for the C_M–R_P–L_P network (see Appendix A.2). Subtracting the inductive reactance of L_P from the capacitive reactance of C_M leaves a total capacitive series reactance for the C_M–R_P–L_P network of 231 Ω. Using the conversion of Eq. (4), the equivalent parallel resistance is found to be 7630 Ω. The equivalent parallel resistance for the sample coil is the product of its Q of 50 and its inductive reactance of 27 Ω, for a value of 1350 Ω. The parallel combination of 7630 Ω and 1350 Ω is 1147 Ω. The resulting Q is 42, i.e., higher than the normal matched Q of 25, leading to bandwidths of 1.03 MHz and 1.73 MHz for the mismatched (considered here) and matched case, respectively, in good agreement with the results of the simulations. However, we note that the formulas used for the calculations are high-Q approximations (see Appendix A.2) and thus we suspect the simulations in principle to closer reflect an experimental result. Of course, for an actual NMR probe we cannot assume that a Varian preamp can be placed close to the matching capacitor. However, $n\lambda/2$ cables have the impedance transformation property that the impedance is unchanged. Therefore, if an $n\lambda/2$ cable is used to connect the preamp and the probe, the above analysis will still be valid. Note that the cable length must be measured from the Varian preamplifier "PROBE" port to the probe's matching capacitor, and not to the RF connector at the base of the probe.

The situation described above is clearly undesirable for spectra having very wide bandwidths, since the probe/preamplifier bandwidth has been reduced by nearly a factor of two from what would be obtained for the typical 50 Ω preamplifier input impedance. We may ask if there is some way to recover the lost bandwidth, and we recall that for our initial analysis, we constrained the length L of the transmission line to be $n\lambda/2$ where $n = 0, 1, 2 \ldots$ It seems natural to think of adjusting the length of the transmission line (TL) in order to minimize the parallel resistance presented by the C_M–R_P–L_P network, although we should now call this the C_M–TL–R_P–L_P network. If we look back at the formula for equivalent parallel resistance, it is clear that to minimize $R_{parallel}$ we need to minimize X_{series}. This simply means we need to find a length of the transmission line that results in a series resonant combination of C_M–TL–L_P, i.e., $X_{series} = 0$ which leaves $R_{parallel} = R_{series} = 7\ \Omega$. Using a transmission line of optimal length, we can expect a significant improvement in bandwidth even beyond that obtained with a 50 Ω preamplifier. This stratagem has previously been suggested by Suddarth to improve the bandwidth of superconductive NMR probes [31]. By taking this route we violate one of the assumptions underlying our analysis, that

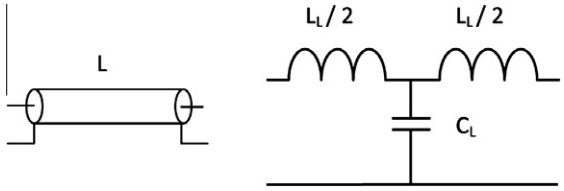

Fig. 10. A "T"-model lumped element circuit, which may serve as an approximation for a transmission line *L*.

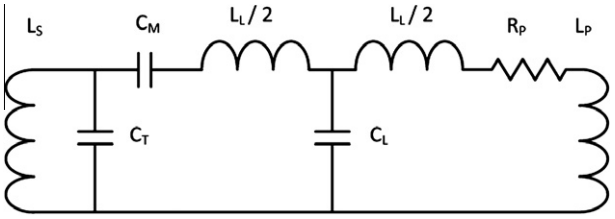

Fig. 11. Electronic circuit obtained by substitution of the "T"-model lumped element circuit in Fig. 10 for the transmission line *L* in Fig. 9.

the impedance of the load (i.e., the cables and preamplifier) can be considered to be constant across the bandwidth of the spectrometer, because we have introduced a second resonance, very close to the original resonance. We can indeed broaden the bandwidth significantly, but we can no longer expect the spectrometer's response to have a simple Lorentzian shape.

We consider how to represent this circuit for conceptual purposes. A helpful approach is to resort to a lumped element approximation for the transmission line. In this case, a "T" model may be the most useful. We can approximate the continuous line by an inductor that has its capacitance to ground lumped into the center (Fig. 10). With this representation we can see more clearly that the circuit can be thought of as two resonant *LC* networks coupled together (Fig. 11). The second resonance derives from the parallel combination of $L_L/2 + L_P$ with C_L. This tank circuit is coupled to the probe through the series combination of C_M and the other $L_L/2$. Because the frequency of the second resonance depends on the length *L* of the transmission line, we can expect the system response to be very sensitive to *L* in the neighborhood of the optimal bandwidth. It may not be sufficient to calculate the required length of the transmission line from first principles. Instead, it is better to couple a small swept test signal into L_S and observe it at the output of the preamplifier – or perhaps the spectrometer, if a general-purpose network analyzer is not available for this test. The length of the transmission line can be adjusted until the bandwidth maximum is reached. The shape of the response will not be Lorentzian, so if quantitative analysis is required it may be worthwhile to record the measured response.

For the Varian preamp and triple-resonance probe system (see Section 2), the probe was found to have a *Q* of 50, which should (for a 50 Ω preamp) lead to a −3 dB bandwidth of 0.866 MHz. However, different lengths of cable *L* were found to result in a range of bandwidths as illustrated in Fig. 12. Length 1 (red) produced a −3 dB bandwidth of 3.70 MHz, which is sufficient for most applications, while Length 2 (green) led to a −3 dB bandwidth of about 0.50 MHz, which appears insufficient for many applications in ^{14}N MAS NMR. The tilted "doublet-type" curve for the cable Length 1 and observed for cable lengths in the region corresponding to the wide bandwidth regime is most likely responsible for the tilt observed experimentally in for example the ^{14}N MAS NMR spectra in Fig. 2 or elsewhere [4]. Thus, it is clear that a correct choice of cable length can be of great importance, at least for observation of wide bandwidth NMR spectra of low-γ quadrupolar nuclei.

To investigate the possibility of finding a cable length that results in a gain curve having a flat response over the widest possible bandwidth (i.e., about 4 MHz) and corresponding to the "ideal" spectrum, a series of simulations have been performed using the Eclipse circuit simulator (Arden Technologies, Goode, VA). Thus, several simulations of the system response for the Varian High-Power Preamp (VHPP) connected to a probe through a transmission line of variable length were carried out. The complex reflection and transmission coefficients of the VHPP were measured using an Agilent 8753ES VNA and converted to a "black-box" file for the Eclipse circuit simulator. Selected results from these simulations are shown in Fig. 13. The green trace is the transmission response for the bare probe into a 50-Ω load, while the red and black traces

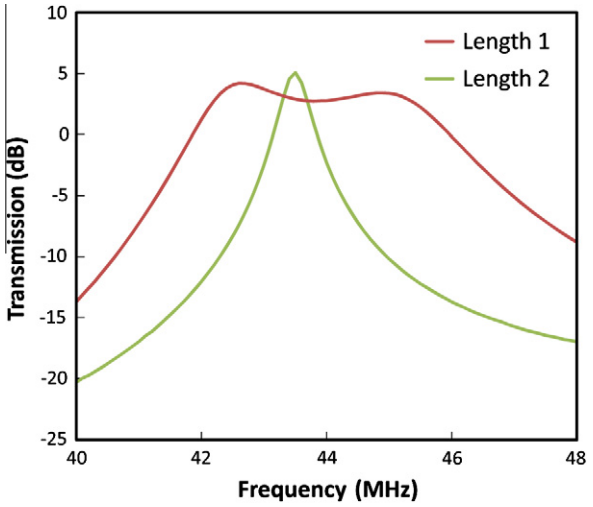

Fig. 12. Bandwidths at 43.3 MHz (^{14}N at 14.1 T) for a Varian triple-resonance probe (*Q* of 50 at 43.3 MHz) connected to a Varian HP preamp using two different lengths of the cable *L* and measured employing the Agilent 8753ES Vector Network Analyzer.

are for the probe → *TL* → VHPP system. The probe *Q* was set to be 100 (unloaded) at 43.3 MHz, which is quite similar to the value $Q \sim 130$ provided by the manufacturer for the Varian/Chemagnetics 7.5 mm T3® CP/MAS probe used in this study. The preamp gain is 43 dB, so the bare-probe curve (green) has been shifted up for comparison with the two system curves. A $TL = 0.185\lambda$ (red curve) broadens and almost completely flattens the system bandwidth, while a $TL = 0.432\lambda$ (black curve) reduces the system bandwidth. Thus, simulations of the system response, using measured parameters of the VHPP, indicate that it is possible to either reduce or enhance the spectrometer bandwidth by varying the length of the cable connecting the probe and preamplifier. For this simulation, we have matched the probe to 50 Ω as is normally done, and we have varied only the cable length. Therefore, there can be no change in the gain or noise figure on resonance. We have shown that the off-resonance gain depends strongly on the length of the cable connecting probe and preamplifier. As Suddarth pointed out [31], the noise figure off-resonance will also be a function of the cable length, and will depend on the parameters of the specific preamplifier used. We have not measured the noise figure of the VHPP as a function of source impedance, and we have not attempted to optimize the noise performance. However, the dependence of preamplifier noise on frequency offset is directly visible in any NMR spectrum. For example, for the spectra in Fig. 3 it is clear the noise level does not depend strongly on frequency. Therefore, it appears that we have achieved this bandwidth enhancement at no real cost to spectrometer noise performance.

We should also note that the adjustment of cable length should not affect transmission bandwidth. The dependence of bandwidth

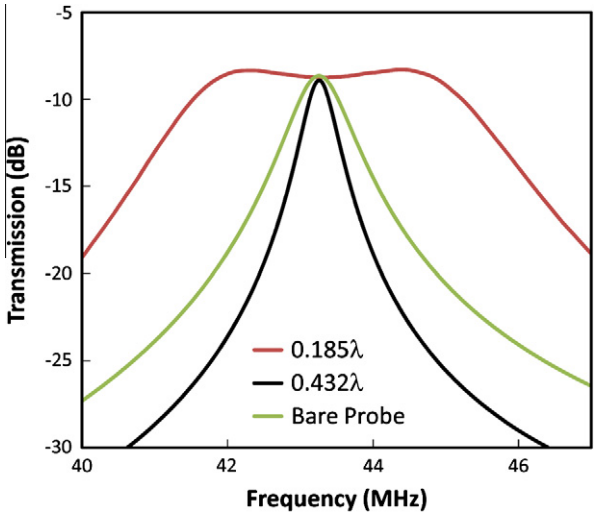

Fig. 13. Bandwidth curves at 43.3 MHz (^{14}N at 14.1 T) selected from a series of simulated curves using the Eclipse circuit simulator for different lengths of the transmission line ($TL = k\lambda$) between a probe Q set to 100 (unloaded) at 43.3 MHz (similar to the Varian/Chemagnetics T3® CP/MAS probe actually used) and the Varian HP preamp (VHHP). In addition, the simulations used the earlier measured complex reflection and transmission coefficients for the VHHP by the Agilent 8753ES VNA, which were converted to a "black-box" file for the Eclipse circuit simulator (see text).

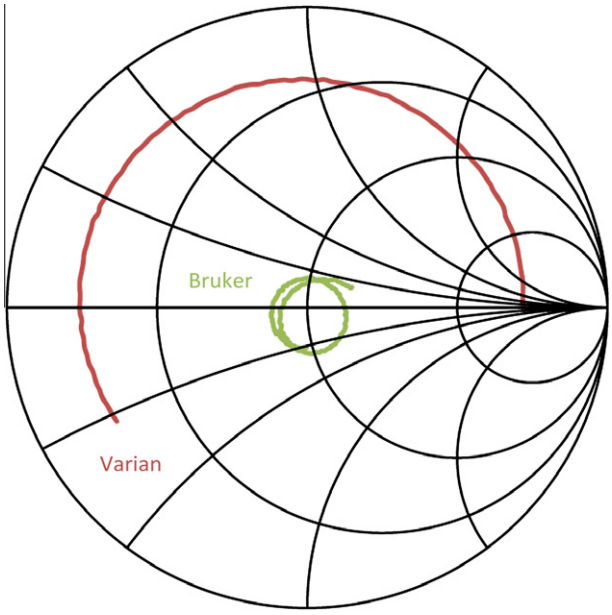

Fig. 14. Smith chart plots illustrating the impedance/reflection coefficients for the Bruker and Varian preamplifiers for a frequency range from 30 to 75 MHz, with both the Bruker "30–75 MHz filter" and the Varian "45–65 MHz $\lambda/4$ cable" in place for their respective preamplifiers. The Smith charts are plots of the input reflection curves observed on the screen of the Agilent 8753ES VNA when turned-on for acquisition of their respective FIDs, and serve as an alternative illustration to the actual electronic measurements performed/reported in the text. *Note*: For reasons of clarity, an overwhelming number of Smith curves and numbers have been omitted in the displayed Smith chart plots. However, we find that research groups, with an interest in this field of solid-state NMR research, are able to correlate the presented very illustrating Smith chart curves with the actual data resulting from the VNA measurements performed for the two different preamplifiers, and presented in the text above.

on cable length is associated with an impedance mismatch between cable and preamplifier. During a transmit pulse, the preamplifier is switched out of the circuit. Assuming that the rf power amplifier output impedance is close to 50 Ω, the transmission bandwidth will be essentially independent of cable length.

We now turn our attention from the above measurements for the parameters of the Varian High-Power Preamplifier (VHPP) to an evaluation of an X-nucleus High-Power (HP) preamp for the Bruker 830-DRX spectrometer. As stated above we measured the input impedance for the VHPP at 43.3 MHz (the ^{14}N frequency for the Varian *Unity* INOVA spectrometer at 14.1 T) and found it to be $7 + j14\ \Omega$, which is quite different from the 50 Ω impedance of the connecting transmission lines. For the Bruker 830-DRX spectrometer we measured the input impedance of the Bruker preamp at 60 MHz to be $46.4 - j13.8\ \Omega$, i.e., quite close to the 50 Ω system impedance. From the experiments and simulations outlined above it was found that the large reflection coefficient for the Varian preamp caused the system bandwidth to depend strongly on probe-to-preamp cable length. We believe that the bandwidth of the Bruker instrument will be nearly independent of cable length.

The measured input impedance/reflection coefficients for the Bruker and Varian spectrometer preamps are shown as Smith chart plots in Fig. 14 for a frequency range from 30 to 75 MHz for both preamps. For these measurements the Bruker preamp has its
"30–75 MHz filter" in place, and the Varian preamp its "45–65 MHz $\lambda/4$ cable". Thus, for both spectrometer systems, the measured configuration matches their normal experimental configuration, however, for the Varian configuration without the standard low-/band-pass filter that would be required in case ^{1}H decoupling is needed. The difference between the two preamps in their performance for low-γ quadrupolar nuclei, as investigated here for ^{14}N at 14.1 T (43.3 MHz) and 19.6 T (60.2 MHz), is striking. The reflection coefficient Γ for the Varian preamp is between about 0.7 and 0.8, while for the Bruker preamp Γ is between about 0.07 and 0.13 over the same frequency range. The cable length between the probe and preamp can therefore be expected to make only a small difference to the bandwidth (*rfbw*) for the Bruker spectrometer. Thus, the bandwidth of the Bruker systems is expected to be determined by the Q of the probe only. Indeed, we performed a series of measurements by injecting a small swept test signal into the 4 mm single-resonance MAS probe (used for the ^{14}N experiments and tuned to 60.2 MHz) for four different cable lengths, which were varied between 0 and 96 cm by addition of separate cables to the standard coaxial cable used between the probe and preamp, and observed the response at the output of the preamplifier. The shape of the responses for these cables (not shown) looks quite similar with only very small differences. Electronic transformations for each of the four response curves to their Q (−3 dB) quality factors, show that the corresponding Q values fall in the range 83 ± 10, which is in excellent agreement with the value of 80 ± 7 determined experimentally for the $Q(=\upsilon_0/rfbw)$ of the probe from simulations of the optimized fitting to the experimental ^{14}N MAS NMR spectra of glycine shown in Figs. 4–7, (i.e., simulations which all correspond to optimized bandwidths in the range $rfbw = 750 \pm 60$ kHz, *vide infra*). At the request of a referee we should note that the S/N ratio of a probe as well as its B_1 rf field strength are proportional to $Q^{1/2}$. This is just as true with an external resistor added (with the purpose of decreasing the Q value of the probe and thereby increasing its bandwidth) as without.

4. Conclusions

The reasons for the large, non-ideal differences observed in acquisition of wide bandwidth solid-state MAS NMR spectra for low-γ nuclei (e.g. ^{14}N), employing the standard experimental setup

for two commercial NMR spectrometers, have been accounted for using electronic measurements and simulations, and traced down to differences in the circuitries for the preamplifiers of the two spectrometers. It is shown that different opportunities exist for obtaining almost ideal wide bandwidth solid-state MAS spectra on both spectrometers (e.g., up to ~4 MHz for ^{14}N at 43.3 MHz on the Varian system) by careful electronic measurements/simulations for the optimum length of the 50 Ω probe-to-preamp cable on the Varian spectrometer and by proper adjustment of the value for the Q of the probe used on the Bruker spectrometer. Finally, these considerations not only apply to the acquisition of MAS spectra, but should also be useful and therefore considered when performing static broadband NMR experiments of low-γ nuclei.

Acknowledgments

The use of the facilities at the Instrument Centre for Solid-State NMR Spectroscopy, Aarhus University, sponsored by the two Danish Science Research Councils, Teknologistyrelsen, the Carlsberg Foundation, Direktør Ib Henriksens Foundation is acknowledged. A portion of this work was performed at the National High Magnetic Field Laboratory, which is supported by National Science Foundation Cooperative Agreement No. DMR-0654118, the State of Florida, and the US Department of Energy.

Appendix A. Electronic definitions/calculations related to NMR preamplifiers and probes

A.1. Evaluation of the Varian High-Power (HP) broadband preamplifier and standard MAS NMR probes

The impedance (Z) is composed of a real part, which is the resistance (R), and an imaginary part, which we call the reactance (X). Therefore, we write the impedance as $Z = R + jX$. The reactance of an inductor is positive and is proportional to the inductance L, as $X_L = \omega L$. The reactance of a capacitor is negative and is inversely proportional to the capacitance C: $X_C = -1/(\omega C)$. The measured input impedance of the Varian HP preamplifier at 43.3 MHz (at the "PROBE" port), and with the Varian 45–65 MHz $\lambda/4$ wavelength cable in place, is $Z = 7 + j14\ \Omega$. Thus, we can model the input to the Varian preamplifier as a resistor of 7 Ω in series with an inductor of 51 nH (Fig. 9) according to $X_L = \omega L = 2\pi\nu L = 2\pi \times 43.3 \times 10^6 \times L = 14$, which gives $L = 51.4$ nH. With the proposed $L_S = 100$ nH for the inductance of the sample coil in the probe circuitry tuned to 43.3 MHz (left side of the circuitry in Fig. 9), we obtain $X_L = \omega L = 2\pi \times 43.3 \times 10^6 \times 100 \times 10^9 = 27\ \Omega$. Therefore, since at resonance $X_L + X_C = 0$ or $\omega L - 1/\omega C = 0$ it follows that

$$C = [\omega^2 L]^{-1} = [(2\pi \times 43.3 \times 10^6)^2 \times 100 \times 10^{-9}]^{-1} = 135\ \text{pF} \quad (5)$$

i.e., the total capacitance required for resonance is $C = 135$ pF.

A.2. Parallel equivalents for the series C_M–R_P–L_P network and the sample coil

For the matching capacitor $C_M = 15$ pF the capacitive reactance is calculated as:

$$X_C = [-\omega C]^{-1} = -[2\pi \times 43.3 \times 10^6 \times 15 \times 10^{-12}]^{-1} = -245\ \Omega \quad (6)$$

Thus, the total series reactance of the C_M–R_P–L_P network ($X = X_C + X_L$) is capacitive and equal to 14–245 = −231 Ω. Using the series-to-parallel transformation (Eq. (4) we can determine the parallel equivalents for the C_M–R_P–L_P series network:

$$R_{parallel} = (7^2 + 231^2)/7 = 7630\ \Omega \quad \text{and}$$
$$X_{parallel} = (7^2 + 231^2)/231 = 231\ \Omega \quad (7)$$

In order to determine the equivalent parallel resistance for the sample coil we find it convenient to first introduce: *Some notes on the Q for a sample coil*:

The *loaded* Q of the sample coil, generally measured employing a spectrum or network analyzer or using the spectrometer "Q-tune", is half the value of that for the *unloaded* Q (which can also be measured using more specialized techniques).

Case (1): If we consider the coil resistance R to be in series with inductance L, then the coil impedance $Z_L = R + j\omega L$ and the quality factor $Q = \omega L/R$. Thus, for this case we have

$$Z_L = R + j\omega L = (\omega L)/Q + j\omega L = \omega L(1/Q + j) \quad (8)$$

i.e., $Z_L \approx j\omega L$ and therefore the impedance is fully inductive.

Case (2): It is possible, and sometimes useful, to transform the series resistance into an equivalent parallel resistance. Assuming the case of a high-Q coil, i.e., $\omega L \gg R$:

$$R_{parallel} = (R_{series}^2 + X_{series}^2)/R_{series} = (0^2 + (\omega L)^2)/R_{series}$$
$$= (\omega L/R_{series}) \times \omega L = Q \times \omega L \quad (9)$$

Therefore, we can now calculate the equivalent parallel resistance for the sample coil as the product of Q(=50) and its inductive reactance $X_L = \omega L = 27\ \Omega$ giving a value of 1350 Ω. Thus, it follows that the parallel combination of these two resistors gives

$$R^{-1} = 7630^{-1} + 1350^{-1} = 8.718 \times 10^{-4}\ \Omega^{-1} \quad \text{or } R = 1147\ \Omega \quad (10)$$

and the resulting Q for this mismatched case has increased to $Q = 42$ ($Q = 50 \times 1147/1350 = 42$) compared to the normal matched $Q = 25$ ($Q = 50 \times 675/1350 = 25$), where the parallel combination corresponds to the two resistors are of equal magnitude and therefore

$$R^{-1} = 1350^{-1} + 1350^{-1} = 14.81 \times 10^{-4}\ \Omega^{-1} \quad \text{or } R = 675\ \Omega \quad (11)$$

For the mismatched case considered here this leads to a bandwidth $rfbw = 43.3/42 = 1.03$ MHz which should be compared to the bandwidth $rfbw = 43.3/25 = 1.73$ MHz for the matched case. Both values are in good agreement with the results of the circuit simulations shown above in the standard text (1.01 MHz and 1.75 MHz, respectively).

References

[1] H.J. Jakobsen, H. Bildsøe, J. Skibsted, T. Giavani, ^{14}N MAS NMR spectroscopy: the nitrate ion, J. Am. Chem. Soc. 108 (2001) 5098–5099.
[2] T. Giavani, H. Bildsøe, J. Skibsted, H.J. Jakobsen, ^{14}N MAS NMR spectroscopy and quadrupole coupling data in characterization of the IV ↔ III phase transition in ammonium nitrate, J. Phys. Chem. B 106 (2002) 3026–3032.
[3] T. Giavani, K. Johannsen, C.J.H. Jacobsen, N. Blom, H. Bildsøe, J. Skibsted, H.J. Jakobsen, Unusual observation of nitrogen chemical shift anisotropies in tetraalkylammonium halides by ^{14}N MAS NMR spectroscopy, Solid State Nucl. Magn. Reson. 24 (2003) 218–235.
[4] T. Giavani, H. Bildsøe, J. Skibsted, H.J. Jakobsen, A solid-state ^{14}N magic-angle spinning NMR study of some amino acids, J. Magn. Reson. 166 (2004) 262–272.
[5] T. Giavani, H. Bildsøe, J. Skibsted, H.J. Jakobsen, Determination of nitrogen chemical shift anisotropy from the second-order cross-term in ^{14}N MAS NMR spectroscopy, Chem. Phys. Lett. 377 (2003) 426–432.
[6] B. Zhou, T. Giavani, H. Bildsøe, J. Skibsted, H.J. Jakobsen, Structure refinement of $CsNO_3$(II) by coupling of ^{14}N MAS NMR experiments with WIEN2k DFT calculations, Chem. Phys. Lett. 402 (2005) 133–137.
[7] H.J. Jakobsen, A.R. Hove, R.G. Hazell, H. Bildsøe, J. Skibsted, Solid-state ^{14}N MAS NMR of ammonium ions as a spy to structural insights for ammonium salts, Magn. Reson. Chem. 44 (2006) 348–356.
[8] A.R. Hove, H. Bildsøe, J. Skibsted, M. Brorson, H.J. Jakobsen, Probing crystal structures and transformation reactions of ammonium molybdates by ^{14}N MAS NMR spectroscopy, Inorg. Chem. 45 (2006) 10873–10881.
[9] H.J. Jakobsen, A.R. Hove, H. Bildsøe, J. Skibsted, M. Brorson, Long-term stability of rotor-controlled MAS frequencies to 0.1 Hz proved by ^{14}N MAS NMR experiments and simulations, J. Magn. Reson. 185 (2007) 159–163.
[10] L.A. O'Dell, R.W. Schurko, WURST-QCPMG static solid-state ^{14}N NMR of KNO_3, J. Am. Chem. Soc. 131 (2009) 6658–6659.
[11] L.A. O'Dell, R.W. Schurko, Static solid-state ^{14}N NMR and computational studies of nitrogen EFG tensors in some crystalline amino acids, Phys. Chem. Chem. Phys. 11 (2009) 7069–7077.

[12] L.A. O'Dell, R.W. Schurko, K.J. Harris, J. Autschbach, C.I. Ratcliffe, Interaction tensors and local dynamics in common structural motifs of nitrogen: a solid-state and DFT study, J. Am. Chem. Soc. 133 (2011) 527–546.
[13] Z. Gan, Measuring amide nitrogen quadrupolar coupling by high-resolution $^{14}N/^{13}C$ NMR correlation under magic-angle spinning, J. Am. Chem. Soc. 128 (2006) 6040–6041.
[14] S. Cavadini, A. Lupulescu, S. Antonijevic, G. Bodenhausen, Nitrogen-14 NMR spectroscopy using residual dipolar splittings in solids, J. Am. Chem. Soc. 128 (2006) 7706–7707.
[15] S. Cavadini, S. Antonijevic, A. Lupulescu, G. Bodenhausen, Indirect detection of nitrogen-14 in solids via protons by nuclear magnetic resonance spectroscopy, J. Magn. Reson. 182 (2006) 168–172.
[16] Z. Gan, Rotary resonance echo double resonance for measuring heteronuclear dipolar coupling under MAS, J. Magn. Reson. 183 (2006) 235–241.
[17] S. Cavadini, S. Antonijevic, A. Lupulescu, G. Bodenhausen, Indirect detection of nitrogen-14 in solid-state NMR spectroscopy, ChemPhysChem 8 (2007) 1363–1374.
[18] Z. Gan, $^{13}C/^{14}N$ heteronuclear multiple-quantum correlation with rotary resonance and REDOR dipolar recoupling, J. Magn. Reson. 184 (2007) 39–43.
[19] Z. Gan, J. Amoureux, J. Trebosc, Proton-detected ^{14}N MAS NMR using homo-nuclear decoupled rotary resonance, Chem. Phys. Lett. 435 (2007) 163–169.
[20] S. Cavadini, A. Abraham, G. Bodenhausen, Proton-detected nitrogen-14 NMR by recoupling of heteronuclear dipolar interactions using symmetry-based sequences, Chem. Phys. Lett. 445 (2007) 1–5.
[21] Z. Gan, Measuring nitrogen quadrupolar coupling with ^{13}C detected wide-line ^{14}N NMR under magic-angle spinning, Chem. Commun. (2008) 868–870.
[22] S. Cavadini, A. Abraham, G. Bodenhausen, Coherence transfer between spy nuclei and nitrogen-14 in solids, J. Magn. Reson. 190 (2008) 160–164.
[23] S. Cavadini, V. Vitzthum, S. Ulzega, A. Abraham, G. Bodenhausen, Line-narrowing in proton-detected nitrogen-14 NMR, J. Magn. Reson. 202 (2010) 57–63.
[24] A.K. Khitrin, B.M. Fung, ^{14}N nuclear magnetic resonance of polycrystalline solids with fast spinning at or very near the magic angle, J. Chem. Phys. 111 (1999) 8963–8969.
[25] Z. Gan, private communication.
[26] Z. Gan, P.L. Gor'kov, W.W. Brey, P.J. Sideris, C.P. Grey, Enhancing MQMAS of low-γ nuclei by using a high B_1 field balanced probe circuit, J. Magn. Reson. 200 (2009) 2–5.
[27] A. Samoson, Satellite transition high-resolution NMR of quadrupolar nuclei in powders, Chem. Phys. Lett. 119 (1985) 29–32.
[28] H.J. Jakobsen, J. Skibsted, H. Bildsøe, N.C. Nielsen, Magic-angle spinning NMR spectra of satellite transitions for quadrupolar nuclei in solids, J. Magn. Reson. 85 (1989) 173–180.
[29] Varian Manual, STARS (SpecTrum Analysis for Rotating Solids) User's Guide, Publication No. 87-195233-00, Rev. A0296, 1996.
[30] S. Anferova, V. Anferov, M. Adams, P. Blumler, N. Routley, K. Hailu, K. Kupferschlager, M.J.D. Mallett, G. Schroeder, S. Sharma, B. Blumich, Construction of a NMR-mouse with short dead time, Concepts Magn. Reson. 15 (2002) 15–27.
[31] S. Suddarth, A method for matching high-temperature superconductor resonators used for NMR signal pickup at 400 MHz, IEEE Trans. Biomed. Eng. 45 (1998) 1061–1066.